# Toward quantification of strain-related mosaicity in shocked lunar and terrestrial plagioclase by *in situ* micro-X-ray diffraction

**Annemarie E. Pickersgill[1*†], Roberta L. Flemming[1], and Gordon R. Osinski[1,2]**
[1]Dept. of Earth Sciences and Centre for Planetary Science and Exploration, University of Western Ontario, 1151 Richmond St., London, Ontario, N6A 5B7, Canada
[2]Dept. of Physics and Astronomy, The University of Western Ontario, 1151 Richmond St., London, Ontario, N6A 5B7, Canada

[*] Corresponding author. E-mail: a.pickersgill.1@research.gla.ac.uk
[†] Current address: School of Geographical & Earth Sciences, University of Glasgow, Gregory Building, Lilybank Gardens, Glasgow G12 8QQ, U.K.

**Abstract –** Studies of shock metamorphism of feldspar typically rely on qualitative petrographic observations, which, while providing invaluable information, can be difficult to interpret. Shocked feldspars, therefore, are now being studied in greater detail by various groups using a variety of modern techniques. We apply *in situ* micro-X-ray diffraction (µXRD) to shocked lunar and terrestrial plagioclase feldspar in order to contribute to the development of a quantitative scale of shock deformation for the feldspar group. Andesine and labradorite from the Mistastin Lake impact structure, Labrador, Canada, and anorthite from Earth's moon, returned during the Apollo program, were examined using optical petrography and assigned to subgroups of the optical shock level classification system of Stöffler (1971). Two-dimensional µXRD patterns from the same samples revealed increased peak broadening in the chi dimension ($\chi$), due to strain-related mosaicity, with increased optical signs of deformation. Measurement of the full width at half maximum along $\chi$ (FWHM$\chi$) of these peaks provides a quantitative way to measure strain-related mosaicity in plagioclase feldspar.

## INTRODUCTION

Studies of shocked minerals from meteorites, terrestrial impact craters, and returned lunar samples have answered many questions regarding the expulsion history of meteorites, the formation of impact craters, and processes that have affected not only the surface of the Moon, but the surface of the other rocky planets as well. In terrestrial samples, the “go-to” mineral for shock barometry is quartz (e.g., Schneider and Hornemann 1976; Ferrière et al. 2009; French and Koeberl 2010; Fritz et al. 2011), as it is optically simple, resistant to alteration, and present in many common crustal rocks. As a result, the effects of shock metamorphism on quartz have been extensively studied and it is an excellent tool by which to determine pressure history of shock-metamorphosed rocks. However, in many of the systems listed above, such as meteorites, the surface of the Moon, and the surface of Mars, quartz is much less prevalent than it is on Earth. One of the most promising but understudied minerals for shock barometry, in the absence of quartz, is the feldspar group, particularly the plagioclase series, which is nearly ubiquitous in most planetary systems.

Thus far, studies of shock effects in the feldspar group have been limited, due to their relatively complex crystal structures and the rapid rate at which they weather, making them difficult to study using conventional optical techniques (e.g., French and Koeberl 2010; Pickersgill et al. 2015). As a result, the effects of shock on feldspar are being increasingly investigated using a wider range of investigative techniques such as Raman spectroscopy (e.g., Fritz et al. 2005; Jaret et al. 2014), cathodoluminescence (e.g., Gucsik et al. 2004; Kayama et al. 2012), and now micro-X-ray diffraction (μXRD). In X-ray diffraction (XRD) studies, increased strain causes peak broadening in the 2-theta (2θ) direction (Fig.1) due to progressive deformation of the crystal lattice and the resultant variation in d-spacing of the crystal. At pressures lower than those that cause peak broadening in 2θ, deformation of the crystal as a result of non-uniform pressure is also seen through the existence of multiple closely related diffracting subdomains, termed strain-related mosaicity. Strain-related mosaicity is evidenced in micro- and single-crystal XRD studies as an extension or streaking of the pattern along the Debye rings (chi (χ) direction) (Fig. 1). Lengthening along the χ direction progresses from single equant spots (undeformed), to short streaks, to longer streaks, to short rows of spots (asterism) with increasing pressure, ultimately to full rings (polycrystalline due to pulverization) or amorphous bands (due to pressure-related amorphization) (Hörz and Quaide 1973; Flemming 2007; Izawa et al. 2011; Vinet et al. 2011). *In-situ* micro-X-ray diffraction (μXRD) has immense value over destructive techniques for examining precious planetary materials. This contribution adds to the growing body of knowledge about shock in feldspars, using μXRD to quantify the level of strain-related mosaicity experienced by shock-metamorphosed plagioclase feldspar through measurement of the full-width-at-half-maximum (FWHMχ) of streaks in degrees chi (°χ) and correlation with optically derived signs of shock metamorphism. This is a technique that has been previously applied successfully to study strain-related mosaicity in enstatite (Izawa et al. 2011) and olivine (McCausland et al. 2010; Vinet et al. 2011), but is being applied to plagioclase for the first time in this work.

# GEOLOGICAL SETTING

## Mistastin Lake impact structure

The Mistastin Lake impact structure is located in central Labrador, Canada (55°53'N; 63°18'W). It is a complex crater structure of approximately 28 km diameter (Grieve 2006). Mak et al. (1976) provide a whole rock $^{40}Ar/^{39}Ar$ age of 36 ± 4 Ma. Its hypervelocity impact origin was confirmed by Taylor and Dence (1969) through the discovery of planar deformation features (PDFs) in quartz and feldspar, diaplectic quartz and feldspar glasses, and poorly developed shatter cones. The structure is located within the Mistastin Lake batholith, which is composed of three main lithologies: anorthosite, granodiorite, and a pyroxene-rich quartz monzonite (sometimes called mangerite) (Currie 1971; Emslie and Stirling 1993). While all three lithologies are feldspar rich, both the granodiorite and the monzonite are heavily weathered and prone to alteration, while the anorthosite has remained relatively unaltered. It is the presence of this large anorthosite body that makes the Mistastin Lake structure an excellent scientific lunar analogue, as anorthosite is also the main constituent of the lunar highlands.

## Apollo Landing sites

Earth's moon is our nearest planetary neighbor, and preserves a rich and extended geological history, due to minimal erosion and lack of crustal recycling. It is a primary exploration target for space agencies the world over and the only planetary body, other than Earth, from which samples have been purposefully collected and returned. Between 1969 and 1972, six Apollo missions returned 2196 individual samples (381.7 kg) from the near-side surface of the Moon (Hiesinger and Head 2006). Samples from five of these missions (11, 12, 15, 16, and 17) were used in this study. A brief summary of the geological setting of each mission's landing site is given below.

Apollo 11 (July 1969) landed at Mare Tranquilitatis (0.7°N, 24.3°E) and largely collected basalt samples but also included pieces of anorthosite that are interpreted to be from the nearby highlands. The majority of samples collected at this location are interpreted to be ejecta from West Crater (Beaty and Albee 1978).

Apollo 12 (November 1969) landed in southeastern Oceanus Procellarum (3.2°N, 23.4°W), near the Surveyor 3 landing site. This site is interpreted to be younger than the Apollo 11 site, based on the relative abundance of craters. At this location there is a relatively thin layer of basalt over non-mare lithologies (Head 1977; Hiesinger and Head 2006). Non-volcanic rocks here originate from a prominent ray from Copernicus crater, which crosses the landing site. The majority of the samples collected from this site are basalts (Hiesinger and Head 2006).

Apollo 15 (July-August 1971) landed in the Hadley-Apennine region (26.1°N, 3.7°E). Samples were collected from the massifs and highlands of the Imbrium rim, and mare of Palus Putredinis (Hiesinger and Head 2006). The site is largely basalts, overlain by rays from Autolycus and Aristillus craters. Both mare and non-mare rocks were collected here, including two types of lava, anorthosites, plutonic rocks, impact melt rocks, granulites, and regolith breccias.

Apollo 16 (May 1972) landed near Descartes Crater (9°S, 15.5°E) in the lunar highlands, the only true highland landing site of the Apollo program (Hiesinger and Head 2006). There are numerous overlapping craters at this site. As a result, all of the returned samples are impactites, most are impact melt rocks or fragmental breccias, with some anorthosite samples. Samples from this site are largely interpreted to be ejecta from the Imbrium, Serenitatis, and Nectaris basin forming events (e.g., Spudis 1984; Haskin et al. 2002).

Apollo 17 (December 1972) landed at the Taurus-Littrow Valley (20.2°N, 30.8°E). This site is at the highland/mare boundary near the southeastern rim of the Serenitatis basin. Samples collected from this site include basalts, impact melt rocks (either from Serenitatis, or Imbrium), and plutonic rocks (Head 1974; Haskin et al. 2002; Hiesinger and Head 2006; Spudis et al. 2011).

**METHODS AND SAMPLES**

Thirty-one polished thin sections from Mistastin Lake were selected from samples collected during three field seasons (2009–2011) (Pickersgill et al. 2015). The selected samples are mainly anorthosite or monomict anorthosite breccia. Grains selected for µXRD were purposely chosen to display the widest possible range of shock metamorphic effects based on the petrographic study outlined in Pickersgill et al. (2015).

Twenty-two polished thins sections from lunar samples were selected from those returned from Apollo missions 11, 12, 15, 16, and 17. Sample selection was based on proportion of plagioclase contained within each thin section, as determined from a literature review, review of the lunar sample catalogue, and inspection of prospective samples at the NASA Johnson Space Centre. The samples are mainly anorthosite, but some gabbro, basalt, impact melt rock, and breccia are also included (see Table 1). Samples were specifically selected to collect the widest possible range of optical deformation (shock effects).

All lunar plagioclase grains observed were perfect structural matches for anorthite by µXRD, an observation which agrees with reported compositions of $An_{89-99}$ for these samples (e.g., Steele and Smith 1973; Dixon and Papike 1975; Warren and Wasson 1977, 1978; Warren et al. 1982). Plagioclase grains from Mistastin matched µXRD patterns of andesine and labradorite, with composition confirmed by EPMA analyses of $An_{31-49}$ (andesine) and $An_{50-55}$ (labradorite) (Pickersgill et al. 2015).

Polished thin sections were examined for microscopic shock metamorphic effects, using a Nikon Eclipse LV100POL compound petrographic microscope, as described in Pickersgill et al. (2015). Micro-X-ray diffraction (µXRD) analyses were performed on individual grains in polished thin sections at the Department of Earth Sciences at The University of Western Ontario, Canada, using a Bruker D8 Discover diffractometer with theta-theta instrument geometry, which enabled the sample to remain horizontal and stationary while the source and detector were rotated. The geometry of the machine results in only reflected X-rays being detected. It has a sealed Cobalt source (CoKα: λ = 1.7889 Å), Gobel mirror parallel beam optics, an exchangeable pinhole collimator (100 or 300 µm), and two-dimensional (2-D) General Area Detector Diffraction System (GADDS). Omega scans were used, wherein the source and detector were rotated simultaneously, both clockwise, through a specified number of degrees (Omega angle, °ω) to simulate rotation of the sample. Counting time was 30 minutes for GADDS frame 1 ($\theta_1$=14.5°, $\theta_2$=16°, ω=6°) and 45 minutes for GADDS frame 2 ($\theta_1$=30°, $\theta_2$=40°, ω=23°). The fraction of the total χ-ring detected varies with the settings for each frame, resulting in a detection limit of 104°χ for Frame 1 and 49°χ for Frame 2. Beam diameter was nominally 300 µm for the majority of samples, and 100 µm for the remainder. Where the same spots were run using each beam diameter, there was no significant difference in the resulting FWHMχ measurements. Large grains of plagioclase (generally >300 µm) were selected for analysis in order to ensure that the X-ray beam was interacting with only (or mainly) the chosen grain, enabling optically observed signs of strain-related mosaic spread (undulose extinction) to be directly correlated with µXRD patterns. This allowed for observation of the same effect with two different techniques, enabling quantification of optical observations of strain-related mosaicity.

Using 2-D GADDS images, spots or streaks were integrated along the length of the Debye rings (chi dimension, $\chi$). The resulting lineshapes had their background subtracted and were smoothed by a factor of 0.15 using a Savitzky-Golay algorithm (Savitzky and Golay 1964) to reduce interference of the noise on measuring the full width at half maximum along $\chi$ (FWHM$\chi$) (Fig. 1). Streak length was quantified by measuring FWHM$\chi$ of each peak using Bruker AXS DiffracPLUS EVA software (Bruker-AXS 2010) in the manner of Izawa et al. (2011). In cases of asterism, the FWHM$\chi$ of each individual peak along the Debye ring was measured and then the individual values for a single set were summed to reconstruct the width of the original peak prior to subdomain formation, as a proxy for the original strain-related mosaic spread, in the manner of Vinet et al. (2011). Data smoothing and FWHM$\chi$ measurement functions are built-in operations of the Bruker AXS DiffracPLUS EVA software. Further details on the µXRD and FWHM$\chi$ technique and are given by Flemming (2007), Izawa et al. (2011), and Vinet et al. (2011).

Error in the FWHM$\chi$ value comes from a systematic measurement error of ±0.01 °$\chi$, based on the measurement resolution of the software, and from the signal to noise ratio, based on the crystallinity of the sample and the diffraction run-time. Signal to noise error was calculated by measuring the FWHM$\chi$ with the baseline at three different locations: the top of the noise, the middle of the noise, and the bottom of the noise. The difference between the maximum/minimum measured FWHM$\chi$ and the middle FWHM$\chi$ was taken for the positive/negative error, respectively. Error is reduced to near 0 with high signal to noise ratio, as observed with high-intensity spots or streaks. However, intensity decreases with increased strain-related mosaicity (increased streak length), so that longer streaks tend to have a lower signal to noise ratio and, therefore, greater error associated with the measurement of the FWHM$\chi$. The average error is less than 0.5°, with the maximum error being 2.5°.

Observed lattice planes were indexed using the following ICDD cards: 01-079-1148 (C)-Andesine; 00-041-1486 (*)-Anorthite; and 01-083-1417 (C)-Labradorite. Eight Miller indices (equal to unique values of 2θ) were analyzed in total: ($\bar{2}$02) = 25.6° 2θ, (004) = 32.7° 2θ, (1$\bar{5}$2) = 47.2° 2θ, (53$\bar{6}$) = 74.7° 2θ, ($\bar{3}$14) = 41.8° 2θ, (42$\bar{4}$) = 55.4° 2θ, (0$\bar{6}$4) = 58.4° 2θ, and (2$\bar{7}$3) = 73.9° 2θ, these peaks were chosen because they occur the most frequently among all of the collected data.

## RESULTS

A wide variety of optical signs of shock were observed in both Mistastin and Apollo samples, ranging from uniform extinction to full isotropism (diaplectic plagioclase glass). Individual crystals of andesine, labradorite, and anorthite were divided into five groups (A-E) based on common optical indicators of strain (Figs. 2, 3). Letters assigned to the groups intentionally increase from A to E in order of increasing apparent degree of deformation.

The FWHM$\chi$ of streaks from the eight most-commonly-detected Miller indices of andesine, labradorite, and anorthite grains were measured to quantify shock-induced strain-related mosaic spread in a similar manner to that employed for enstatite by Izawa et al. (2011). The results of these measurements are summarized in Fig. 4 and Tables 1 and 2. As there is significant overlap in each group compared, we report only average values, not upper or lower boundaries for each group (Table 2). Measurements from the four most commonly occurring Miller indices are exhibited in Fig. 4.

**Group A – Uniform Extinction**

Grains exhibiting uniform extinction are characterized by the entire grain becoming extinct at the same time on rotation of the stage under cross-polarized light (Fig. 2A). All grains in this group showed low degrees of fracturing, distinctly less than those of other groups. GADDS images of grains in this group clearly show individual spots (Fig. 2A). The average FWHM$\chi$ was 0.67 °$\chi$ for Mistastin Lake, and 0.79 °$\chi$ for Apollo.

**Group B – Slight Undulose Extinction**

Grains exhibiting slightly undulose extinction are characterized by rotation of the stage by only 1 to 2°, causing a wave of extinction to pass through the entire grain (Fig. 2B). Most grains in this group show irregular fracturing. GADDS images of grains in this group show spots which are beginning to streak out into ‘lozenges’ that are slightly longer in the $\chi$ dimension than they are in the 2$\theta$ dimension. The average FWHM$\chi$ was 0.89 °$\chi$ for Mistastin Lake, and 0.93 °$\chi$ for Apollo.

**Group C – Undulose Extinction**

Grains exhibiting undulose extinction are characterized by a wave of extinction passing through the grain on rotation of the stage by ~5 to 30° (Fig. 2C), typical of ‘classic’ undulose extinction. The upper limit to this group is grains that are beginning to show signs of mosaic extinction or ‘mosaicism’, in which waves of extinction pass through different parts of the grain in different directions (appearing ‘patchy’). The majority of these grains exhibit irregular fracturing; approximately half show bent and/or offset twins. GADDS images of grains in this group clearly show streaks, which are much longer than they are wide, and some have begun to show asterism, in which the streaks have resolved into short rows of spots (Fig. 2C). The average FWHM$\chi$ was 1.07 °$\chi$ for Mistastin Lake, and 2.58 °$\chi$ for Apollo.

**Group D – Partially Isotropic**

Grains that have become partially isotropic are characterized by only part of the crystal being optically isotropic, while the remainder remains birefringent under cross-polarized light. In the Apollo samples for this group, there appears to be no crystallographic control on which parts are isotropic (Fig. 3A), meaning that the isotropic areas are not confined by linear or planar elements. In the Mistastin samples, there is generally no apparent crystallographic control on which part of the grain becomes isotropic. Occasionally, however, it is only the alternate twins that are amorphized, leaving the remainder of the crystal birefringent. In these cases, no appreciable difference in chemical composition between twin lamellae was observed (Pickersgill et al. 2015). These grains exhibit irregular fracturing and undulose extinction in the remaining birefringent part. GADDS images of grains in this group show clear streaks (Fig. 3A), very similar to those exhibited by Group C. The average FWHMχ was 2.54 °χ for Mistastin Lake, and 3.14 °χ for Apollo.

**Group E – Diaplectic Glass (Fully Isotropic)**

Grains that have become fully isotropic were not found in any of the Apollo samples examined for this study, but were present in many of the Mistastin thin sections (Fig. 3B). They are characterized by continuous extinction of the *entire* grain on rotation under cross-polarized light, the production of an amorphous X-ray pattern, and a homogenous chemical composition matching that of plagioclase feldspar (Pickersgill et al. 2015). Due to the amorphous pattern produced by µXRD, no streaks or spots occur in the resulting GADDS image (Fig. 3B); as a result no measurement in χ is possible for these samples.

**FWHMχ Measurements**

As seen in Fig. 4, there is significant overlap in FWHMχ between the various groups; however, the maximum values, and the average values, in each optical group, form a general upward trend in both the Apollo and Mistastin suites. Optical groups have been purposely arranged in order of increasing apparent deformation (based on petrographic observations). A deviation in the trend of maximum values is clear in Group C of the Apollo suite, in which the maximum value is nearly twice the maximum value of Group D. However, the average values for Groups C and D are the same within error. In each optical group, the maximum streak length is higher in the Apollo suite than in the Mistastin suite, though the difference is so slight as to be dwarfed by the measurement error in all but Group C. There is significant scatter in Group C in both suites.

The biggest variation in streak length with optical group is apparent in these Miller indices: ($\bar{2}02$), (004), ($1\bar{5}2$), and ($53\bar{6}$) (2θ = 25.6°, 32.7°, 47.2°, and 74.7°, respectively). The Miller indices displayed in Fig. 4 were chosen based on their occurrence in all optical groups. These also showed the widest range in streak lengths (e.g., these indices varied over >1–2° FWHMχ across optical groups). Some indices were not present in every optical group, and these were commonly those with higher integers as part of their Miller index (e.g., ($2\bar{7}3$), ($42\bar{4}$) (2θ = 73.9°, 55.4° respectively)). They have been left out of Fig. 4, but included in the calculations of average FWHMχ values. The paucity of reflections at these points is addressed further in the discussion section.

The average values for FWHMχ are very similar between the Apollo and Mistastin suites (Table 2). There is an overall correlation between increased strain-related mosaicity and increased average streak length in χ (Fig. 4). The variations between sample suites in Groups A and C, however, suggest that further study is required to constrain the significance of these values, including the effects of orientation of the crystal relative to the X-ray beam which is currently under investigation.

Due to the large beam size, relative to the width of most polysynthetic twins, it is apparent that several GADDS images picked up both sets of twins. This is evidenced by repetition of the pattern at lower intensity slightly offset from the higher intensity spots or streaks from the twin occupying the majority of the area with which the beam interacted. In these cases, or when adjacent twins were both analyzed intentionally (in order to determine if alternate twins deform differently from each other under shock conditions), the GADDS images indicate that alternating sets of twins typically exhibit the same amount of strain-related mosaicity as one another. Notable exceptions to this are cases in which alternate twin deformation is optically apparent such as preferential isotropization of alternate twin sets. Preferential alteration of alternate twin lamellae to a zeolite phase has also been observed in samples from Mistastin Lake, and is discussed in detail in Pickersgill et al. (2015).

**DISCUSSION**

As evidenced by Fig. 4, FWHMχ measurements along the Debye rings of $(\bar{2}02)$, (004), $(1\bar{5}2)$, and $(53\bar{6})$ (2θ = 25.6°, 32.7°, 47.2°, and 74.7°, respectively) show a general upward trend with optically observed indicators of increasing shock. Other Miller indices (those which had higher integers as part of their index such as $(\bar{3}14)$, $(42\bar{4})$, $(0\bar{6}4)$, $(2\bar{7}3)$ (2θ = 41.8°, 55.4°, 58.4°, and 73.9°, respectively)) sometimes did not occur in all optical groups, and were most frequently lacking in group D, particularly in the Apollo suite. As a result they graphically appear to have less variation, but this is likely due to the aforementioned fact that several Miller indices are missing entirely from one or more optical groups, and variation between two groups is less apparent than variation between many groups. As a result, only those indices appearing in all (or most) optical groups in both suites have been shown in Fig. 4. We hypothesize that the lack of high Miller indices measured in Group D is a result of eradication of these planes at lower pressures due to increasing destruction of long-range order, as seen by Hörz & Quaide (1973).

The minimum values observed for strain-related mosaicity show similarly-shaped trends of increasing mosaic spread with increasing shock stage across all Miller indices. However, very high 'outlier' strain-related mosaicities are only observed for low 2θ reflections (low Miller index), e.g. $(\bar{2}02)$ and (004), which are more readily detectible using this technique. This is because at high 2θ the detector is restricted to sampling a smaller range of χ angles (The 6 inch detector samples a smaller angular proportion of the cone of diffraction, which has a larger circumference at higher 2θ). Therefore long streaks, as produced by highly shocked samples, will trend outside of the perimeter of the detector and will not be measurable and therefore will be systematically omitted. To minimize this effect, only small 2θ angle lattice planes should be used, where the detector samples a larger proportion of the χ angle and therefore a greater proportion of the streaks will be fully observed within the limit of the detector. Alternatively, reported mosaicity could be considered to be a minimum.

Comparisons of FWHMχ measurements of neighboring twins indicate that adjacent twin sets generally deform in a similar fashion, as evidenced by matching streak lengths from each twin. This suggests that the difference in lattice orientation relative to the shockwave, that allows some twins to isotropize or develop planar deformation features (Taylor and Dence 1969; Stöffler 1966; Jaret et al. 2014; Pickersgill et al. 2015), while leaving others crystalline, occurs over a very narrow range of orientations.

## Scatter in FWHMχ measurements

There is a high degree of scatter in FWHMχ measurements from groups B to D. Scatter seems to increase with increasing apparent optical shock level. There are two possible explanations for this: subjectivity of optical group determination, and orientation of the sample.

*Subjectivity of optical group determination:* The optical groups created for this study were based on observations of commonly occurring characteristics across the 189 grains examined in this study (102 from the Apollo suite, 87 from the Mistastin Lake suite). Overlap in streak lengths is accounted for by the highly gradational difference between categories, such as uniform extinction (Group A) and slight undulose extinction (Group B) and between slight undulose extinction (Group B) and undulose extinction (Group C).

*Orientation of the sample:* As a result of the geometry of µXRD as applied to *in-situ* samples, the possible orientations of the crystal lattice relative to the X-ray beam are necessarily restricted by the orientation of the crystal within the sample and, in the case of thin sections, by the orientation of the crystal relative to the plane of the cut sample surface. This necessarily induces scatter in the measurements, because not only is passage of the shockwave through materials known to be heterogeneous, but there will be an orientational dependence of strain-related mosaicity. As a result, if the X-ray beam is interacting with the crystal lattice *perpendicular* to the direction of maximum non-uniform stress (producing maximum non-uniform strain), the degree of streaking will be more extensive than if the X-ray beam is aligned in the *same* direction as the maximum non-uniform stress. The use of randomly-oriented crystals in this study means that statistically the bulk of the FWHMχ measurements will fall somewhere between this minimum value (X-rays parallel to the direction of non-uniform strain) and the maximum value (X-rays perpendicular to the direction of non-uniform strain). As the crystals are not all oriented in the same way relative to the X-rays, this undoubtedly creates a great deal of scatter in the measured FWHMχ. Simple statistics may also play a role in the scatter of Apollo Group C when compared with Mistastin Group C, as more grains populated this category for Apollo samples (65) than for Mistastin samples (15).

In terms of investigating the degree of scatter within individual grains, several spots were measured in individual grains, however no significant difference was observed. This might be a result of the beam diameter relative to the size of the crystal, because even when the nominal beam diameter is 100 µm, at low angles the footprint can be higher; as a result measurements would often include the whole grain regardless of where the beam is centered.

## Subdivision of the lower end of the shock scale

The wide variation in streak length exhibited by grains within Group C (undulose extinction), particularly in the Apollo sample suite, indicates that there is more variation in strain-related mosaicity as a function of shock level than is apparent using conventional optical microscopy. Micro-X-ray diffraction (µXRD) is therefore an excellent tool by which to subdivide the lower end of the shock scale. This is of particular importance in the case of plagioclase as the most widely-used shock scale for plagioclase currently consists of only essentially three categories: 0 – unshocked; I – undulose extinction, PDFs; II – diaplectic glass (Stöffler 1971). Stöffler et al. (1986) use measurements of the refractive indices of shocked plagioclase from the Shergotty meteorite to gain higher resolution division of maskelynite, however we still have only a limited ability to constrain shock information prior to plagioclase isotropization, although the majority of samples fall into this intermediate zone.

Streak lengthening in χ on 2D µXRD GADDS images displaying strain-related mosaicity demonstrates that there is a wide range of streak lengths displayed by grains which show optically undulose extinction (Group C). While this is not a unique indicator of shock metamorphism, this technique has the potential to enable the subdivision of the low end of the pressure scale due to the large range of streak lengths. A consistent, quantifiable, and easily-applicable system to define the level of undulosity optically is currently lacking. One method could be to record the angular difference between the onset of extinction of the first part of the grain and its completion, as the last part of the grain goes extinct; however, this would also need to take into account the size of the grain in question, as smaller grains would necessarily be rotated to a lesser degree than larger grains, in order to sweep through the entire range of extinction angles.

**Comparison of deformation in lunar and terrestrial plagioclase**

As seen in Fig. 4, the samples from the Apollo suite show much higher degrees of strain-related mosaicity in Group C than those of the Mistastin suite. Our preferred explanation is that the higher degree of strain-related mosaicty in lunar samples, as compared with terrestrial samples, is a result of multiple impacts which undoubtedly affected many of the Apollo samples; whereas, we know that the Mistastin samples have only experienced one impact and that there was no other tectonic activity in the region to account for multiple generations of strain-related mosaicity. With respect to the question of why lunar samples would exhibit higher strain-related mosaicity than terrestrial samples without becoming isotropic (maximum in Group C of Apollo suite is nearly twice that of Group D in Apollo suite), we suggest that the answer may be compositional, as supported by the variation in onset pressure of isotropism in high-Ca vs medium-Ca plagioclase given by Fritz et al. (2011). Apollo samples are anorthite (high-Ca plagioclase); whereas Mistastin samples have compositions from labradorite to andesine (medium-Ca plagioclase). Thus, the increased maxima in Group C of the Apollo suite (Fig. 4) is suggested to be linked to multiple impact events, resulting in higher overall strain, and to the increased Ca content of the Apollo suite as compared to the Mistastin suite. Due to the smaller maximum streak lengths in Group D as compared to Group C in the Apollo suite, we suggest that the partial isotropization of these crystals has relieved enough pressure to allow the remaining birefringent part of the grain to remain relatively unstrained.

## CONCLUDING REMARKS

We have shown that the degree of strain-related mosaicty in plagioclase feldspar can be quantified through the use of *in-situ* micro-X-ray diffraction. One should be mindful, however, that streaking in χ can result from non-uniform strain caused by multiple factors, including endogenic tectonic deformation, and not only by the passage of a shockwave during meteorite impact.

An ideal follow-up would be to experimentally shock each composition of feldspar to various peak pressures and then conduct µXRD and petrographic studies on those samples to calibrate shock effects for each group using known pressures and to compare the results of each group to each other, in order to better understand how shock affects different compositions (and therefore mineral structures) as seen by strain-related mosaicity. Additionally, examining the same spots targeted in this study using additional techniques would provide an excellent additional quantitative dataset with which to compare the µXRD-generated FWHMχ values reported herein. Raman spectra, for example, show increased peak broadening and decreased intensity with increasing shock level (Fritz et al. 2005); if Raman spectra were to be gathered from the same spots as used in this study, the FWHM of the Raman bands could be plotted against the FWHMχ of the µXRD patterns and this might better constrain the groups used in this study, as well as possibly illuminating trends or clusters which are not currently distinguishable. It is possible that a follow-up study of this kind would result in clear natural divisions becoming apparent for the lower end of the shock scale (level I according to Stöffler, 1971).

Pursuant to increasing the statistical reliability of this technique for quantification of shock and shock scale subdivision, measuring more grains may help to constrain which Miller indices are most useful, and to better define ranges of streak lengths for each optical group.

*Acknowledgements* – the Natural Sciences and Engineering Research Council of Canada, the Northern Scientific Training Program, and the Canadian Space Agency are thanked for the generous funding they provided to make this project possible. Marianne Mader, Cassandra Marion, Marc Beauchamp, Alaura Singleton and Rodney Dammeier are thanked for their support in the field and sharing samples from previous field seasons. The Nanofabrication Facility at the University of Western Ontario is thanked for funding and training for using their SEM. The Earth and Planetary Materials Analysis (EPMA) Laboratory, also at Western, is gratefully acknowledged for the EPMA work. CAPTEM and the Lunar Sample Laboratory at Johnson Space Centre are gratefully acknowledged for allocating Apollo samples to us. Fred Hörz and Jörg Fritz are thanked for their helpful and thorough reviews of this paper.

## REFERENCES

Beaty D. W., and Albee A. L. 1978. Comparative petrology and possible genetic relations among the Apollo 11 basalts. *Proceedings of the 9th Lunar and Planetary Science Conference* 359–463.

BrukerAXS, 2010. DIFFRACplus Evaluation Package Release 2010. Bruker AXS, Karlsruhe, Germany.

Currie K. L. 1971. Geology of the resurgent cryptoexplosion crater at Mistastin Lake, Labrador. *Bulletin - Geological Survey of Canada 207*. 62 p.

Dixon J. R., and Papike J. J. 1975. Petrology of anorthosites from the Descartes region of the moon: Apollo 16. *Proceedings of the 6th Lunar Science Conference* 263–291.

Emslie R. F., and Stirling J. A. R. 1993. Rapakivi and related granitoids of the Nain plutonic suite: geochemistry, mineral assemblages and fluid equilibria. *The Canadian Mineralogist* 31: 821–847.

Ferrière L., Morrow J. R., Amgaa T., and Koeberl C. 2009. Systematic study of universal-stage measurements of planar deformation features in shocked quartz: Implications for statistical significance and representation of results. *Meteoritics & Planetary Science* 44: 925–940.

Flemming R. L. 2007. Micro X-ray diffraction (µXRD): A versatile technique for characterization of Earth and planetary materials. *Canadian Journal of Earth Sciences* 44: 1333–1346.
French B. M., and Koeberl C. 2010. The convincing identification of terrestrial meteorite impact structures: What works, what doesn't, and why. *Earth-Science Reviews* 98: 123–170.
Fritz J., Greshake A., and Stöffler D. 2005. Micro-Raman spectroscopy of plagioclase and maskelynite in Martian meteorites: Evidence of progressive shock metamorphism. *Antarctic Meteorite Research* 18: 96–116.
Fritz J., Wünnemann K., Greshake A., Fernandes V. A. S. M., Boettger U., and Hornemann U. 2011a. Shock Pressure Calibration for Lunar Plagioclase. *Proceedings of the 42nd Lunar and Planetary Science Conference*.
Fritz J., Wünnemann K., Reimold W. U., Meyer C., and Hornemann U. 2011b. Shock experiments on quartz targets pre-cooled to 77 K. *International Journal of Impact Engineering* 38:440-445.
Grieve R. A. F. 2006. *Impact structures in Canada*, St. John's, N.L.: Geological Association of Canada. 210 p.
Gucsik A., Ninagawa K., Nishido H., Toyoda S., Tsuchiyama A., Bidló A., and Brezsnyánszky K. 2004. Cathodoluminescence (CL) spectral study of experimentally shock-deformed plagioclase (abstract #9012). In *Workshop on Chondrites and Protoplanetary Disk*. Houston, TX, United States (USA): Lunar and Planetary Institute, Houston, TX.
Haskin L. A., Korotev R. L., Gillis J. J., and Jolliff B. L. 2002. Stratigraphies of Apollo and Luna highland landing sites and provenances of materials from the perspective of basin impact ejecta modeling (abstract #1364). *Proceedings of the 33rd Lunar and Planetary Science Conference.*
Head J. W. 1974. Lunar dark-mantle deposits-Possible clues to the distribution of early mare deposits. *Proceedings of the Fifth Lunar Conference (Supplement 5, Geochimica et Cosmochimica Acta)* 1: 207–222.
Head J. W. 1977. Some geologic observations concerning lunar geophysical models. Edited by Pomeroy J. H., and Hubbard N. J. *NASA Special Publication* 370 (Part 1), 407–416.
Hiesinger H., and Head J. W. 2006. New views of lunar geoscience: an introduction and overview. *Reviews in Mineralogy and Geochemistry* 60: 1–81.
Hörz F., and Quaide W. L. 1973. Debye-Scherrer investigations of experimentally shocked silicates. *The Moon* 6: 45–82.
Izawa M. R. M., Flemming R. L., Banerjee N. R., and McCausland P. J. A. 2011. Micro-X-ray diffraction assessment of shock stage in enstatite chondrites. *Meteoritics & Planetary Science* 46: 638–651.
Jaret S., Kah L. C., and Harris R. S. 2014. Progressive deformation of feldspar recording low-barometry impact processes, Tenoumer impact structure, Mauritania. *Meteoritics and Planetary Science* 49(6):1007-1022.
Kayama M., Nishido H., Sekine T., Nakazato T., Gucsik A., and Ninagawa K. 2012. Shock barometer using cathodoluminescence of alkali feldspar. *Journal of Geophysical Research* 117: E09004.
Mak E., York D., Grieve R. A. F., and Dence M. 1976. The age of the Mistastin Lake crater, Labrador, Canada. *Earth and Planetary Science Letters* 31: 345–357.

McCausland P. J. A., Flemming R. L., and Izawa M. R. M. 2010. Quantitative shock stage assessment in olivine and pyroxene bearing meteorites via *in situ* micro-XRD (abstract #P14C-03). *Proceedings of the American Geophysical Union, Fall Meeting 2010*.

Pickersgill A. E., Osinski G. R., and Flemming R. L. 2015. Shock effects in plagioclase feldspar from the Mistastin Lake impact structure, Canada.

Savitzky A., and Golay M. J. E. 1964. Smoothing and Differentiation of Data by Simplified Least Squares Procedures. *Analytical Chemistry* 36: 1627–1639.

Schneider H., and Hornemann U. 1976. X-Ray investigations on the deformation of experimentally shock-loaded quartzes. *Contributions to Mineralogy and Petrology* 55: 205-215.

Spudis P. D. 1984. Apollo 16 site geology and impact melts: Implications for the geologic history of the lunar highlands. *Proceedings of the 15th Lunar and Planetary Science Conference* C95–C107.

Spudis P. D., Wilhelms D. E., and Robinson M. S. 2011. The Sculptured Hills of the Taurus Highlands: Implications for the relative age of Serenitatis, basin chronologies and the cratering history of the Moon. *Journal of Geophysical Research* 116, E00H03.

Steele I. M., and Smith J. V. 1973. Mineralogy and petrology of some Apollo 16 rocks and fines: General petrologic model of moon. *Proceedings of the 4th Lunar Science Conference* 1: 519–536.

Stöffler D. 1966. Zones of impact metamorphism in the crystalline rocks of the Nördlinger Ries crater. *Contributions to Mineralogy and Petrology* 12: 15–24.

Stöffler D. 1971. Progressive metamorphism and classification of shocked and brecciated crystalline rocks at impact craters. *Journal of Geophysical Research* 76: 5541–5551.

Taylor F. C., and Dence M. R. 1969. A probable meteorite origin for Mistastin Lake, Labrador. *Canadian Journal of Earth Sciences* 6: 39–45.

Vinet N., Flemming R. L., and Higgins M. D. 2011. Crystal structure, mosaicity, and strain analysis of Hawaiian olivines using *in situ* X-ray diffraction. *American Mineralogist* 96: 486–497.

Warren P. H., and Wasson J. T. 1977. Pristine nonmare rocks and the nature of the lunar crust. *Proceedings of the 8th Lunar Science Conference1* 2215–2235.

Warren P. H., and Wasson J. T. 1978. Compositional-petrographic investigation of pristine nonmare rocks. *Proceedings of the 9th Lunar and Planetary Science Conference* 185–217.

Warren P. H., Taylor G. J., Keil K., Marshall C., and Wasson J. T. 1982. Foraging westward for pristine nonmare rocks-Complications for petrogenetic models. *Proceedings of the 12th Lunar and Planetary Science Conference* 21–40.

Young K. E., Hodges K. V, van Soest M. C., and Osinski G. R. 2013. Dating the Mistastin Lake impact structure, Labrador, Canada, using zircon (U-Th)/He thermochronology (abstract #2426). *Proceedings of the 44th Lunar and Planetary Science Conference*.

## FIGURES

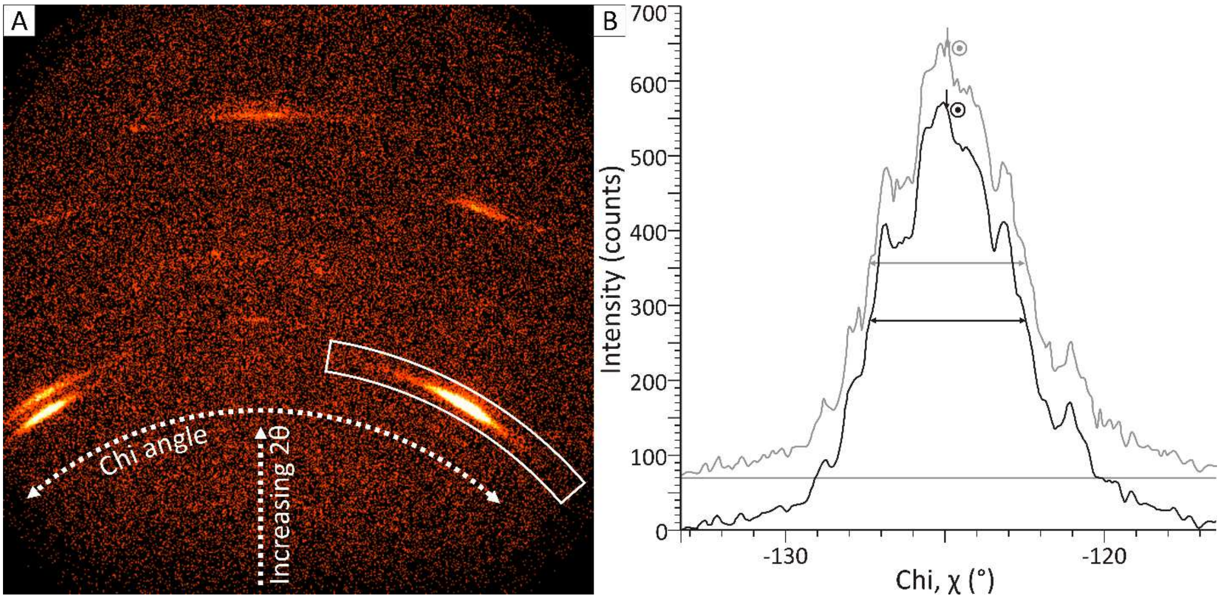


Fig. 1. µXRD GADDS image and stacked plots of intensity vs. °$\chi$. A) µXRD GADDS image of an anorthite crystal in Apollo sample 60015,114. Arrows indicate the direction of $\chi$ and increasing 2$\theta$. White box highlights the streak, which is integrated over a narrow range of 2$\theta$ and plotted as a function of $\chi$, as displayed in (B). B) Stacked plots of intensity vs. °$\chi$ showing raw (grey), smoothed and background subtracted (black) lineshapes, and streak length measurement (FWHM$\chi$) for both. In this case, the raw (grey) FWHM$\chi$ is 4.92° and the processed (black) FWHM$\chi$ is 4.90°.

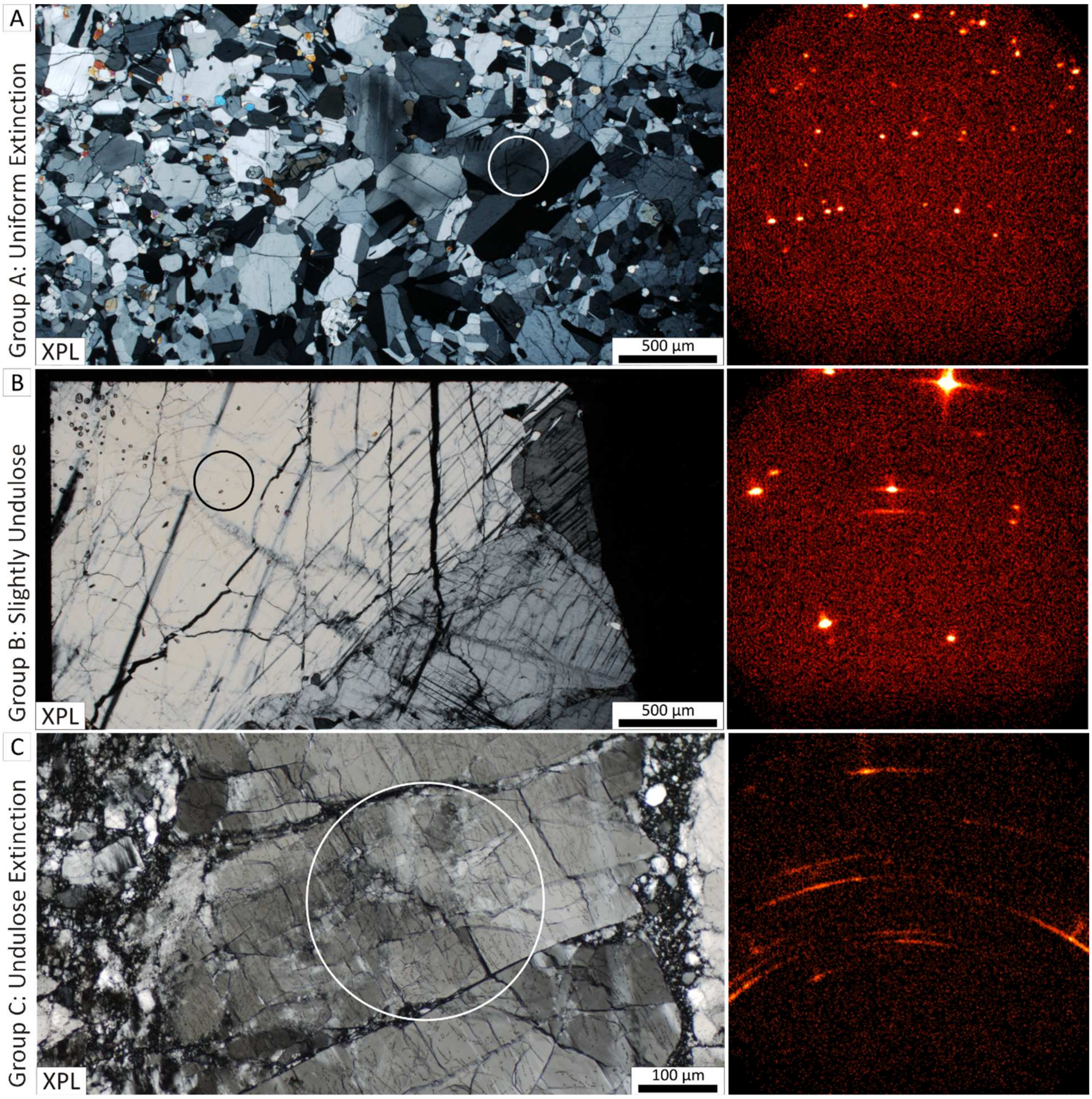


Fig. 2. Representative photomicrographs in cross-polarized light (XPL) of optical groups A-C, correlated with GADDS images from each grain pictured. Note how the pattern on the GADDS images goes from spots (A) to short streaks (B) to long streaks (C). The location of the analysis is indicated by a circle on each image, the circle represents the nominal beam diameter of 300 µm. A) Apollo sample 60619,2 shows uniform extinction under cross polarized light, and spots on the GADDS image. B) Apollo sample 15415,90 shows slight undulose extinction, and the beginning of streaks on the GADDS image in which the bright spots are slightly longer than they are wide – 'lozenge-shaped'. C) Apollo sample 76335,55 shows extremely undulose extinction, bordering on 'mosaicism', and long streaks with the start of asterism on the GADDS image.

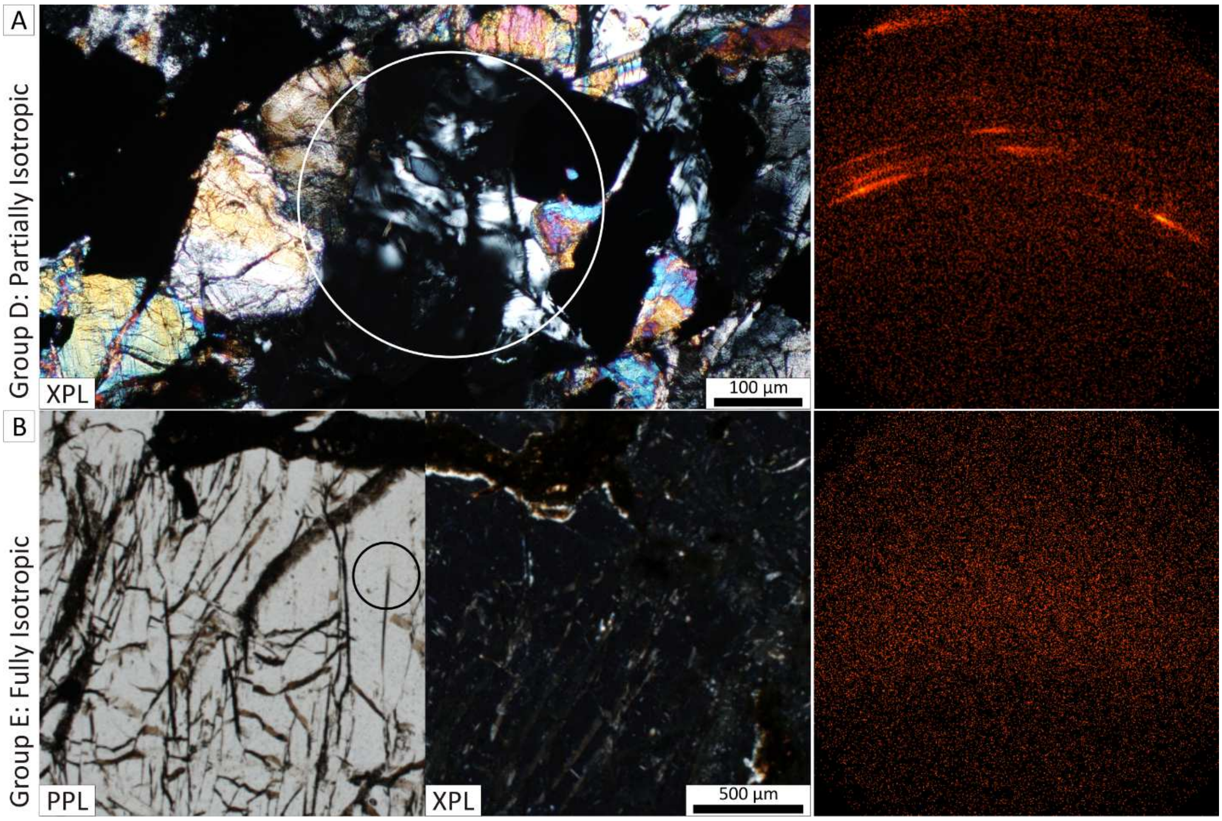


Fig. 3. Representative photomicrographs in cross-polarized light (XPL) of optical groups D and E, correlated with GADDS images from each grain pictured. Note how the pattern on the GADDS images goes from long streaks (A) to an amorphous diffuse band (B). The location of the analysis is indicated by a circle on each image, the circle represents the nominal beam diameter of 300 µm. A) Apollo sample 79155,58 shows a grain which has become partially isotropic (black), while part remains birefringent (centre of circle); the GADDS image, which was centred on the remaining birefringent part of the crystal, shows longer streaks than those in Fig. 2B. B) Mistastin sample MM10-38 has had all plagioclase converted to diaplectic glass. The left photomicrograph shows preservation of textures in plane polarized light and the right image shows total extinction of plagioclase under cross-polarized light. The GADDS image shows a diffuse band through the center of the image, indicative of an amorphous XRD pattern.

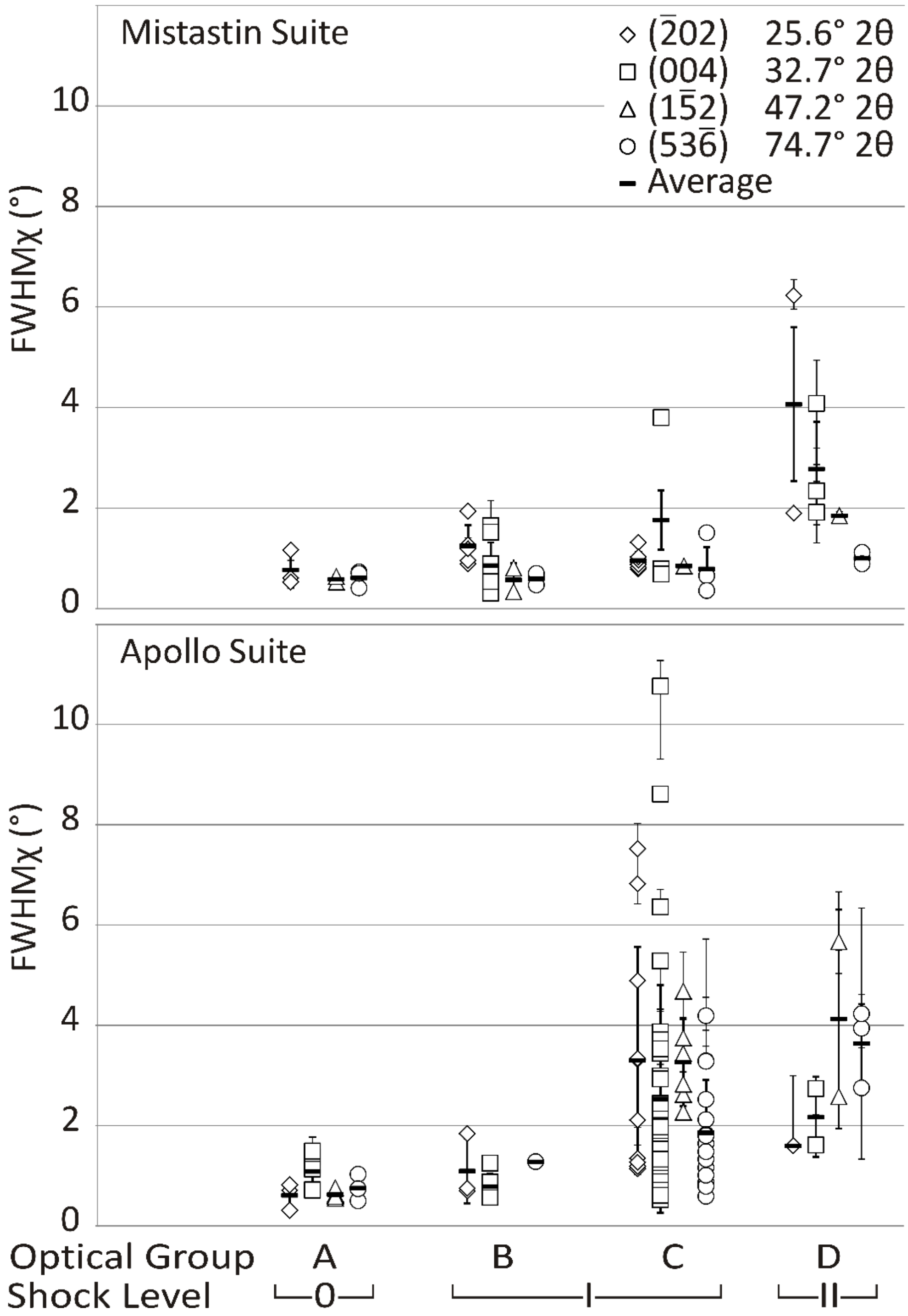


Fig. 4. Graphs of FWHMχ vs. optical group for samples from the Mistastin suite (top) and the Apollo suite (bottom). The four Miller indices displayed (in brackets) are those which are represented in every optical group. Different symbols indicate the Miller index of streaks measured from diffraction of different sets of crystal planes. The average of each set is indicated by a black bar, with bold error bars indicating ± 2σ. A=Uniform extinction; B=Slight undulose extinction; C=Undulose extinction; and D=Grains which have become partially isotropic. Group E (grains which have become fully isotropic) is not shown due to amorphous nature of the µXRD pattern. Also indicated is the shock level of each set according to Stöffler (1971). For clarity, measurements from Miller indices which do not appear in every optical group are not

shown here. Note that in both suites there is a general upward trend from group A to group D (which are arranged in order of increasing apparent optical deformation). In Group C, there is significant difference between FWHM$\chi$ measurements in the Apollo suite as compared to the Mistastin suite. There is significant scatter in the FWHM$\chi$ values for group C in the Apollo suite. Error bars on individual measurements (thin lines) are the difference between the widest/narrowest possible FWHM$\chi$ (baseline set to bottom/top of noise, respectively) and the average FWHM$\chi$ (baseline set to middle of noise).

**TABLES**

Table 1. Apollo sample list: signs of strain; number of grains in each group per thin section; and FWHMχ measurements.

| Sample number | Origin (Apollo mission) | Rock type | Optical effects | | | | | Optical Group (# of grains) | | | | Average FWHM (°χ) |
|---|---|---|---|---|---|---|---|---|---|---|---|---|
| | | | Fracture | Undulose extinction | Mosaicism | Bent twins | Partially Isotropic | A | B | C | D | |
| 10047,16 | Adjacent to LM (11) | Ilmenite basalt | | x | | | | | 1 | | | 0.79 |
| 12054,126 | Surveyor Crater (12) | Ilmenite basalt | x | x | | | | | | 2 | | 6.19 |
| 15362,11 | Spur Crater (15) | Anorthosite (F) | x | x | | | | | 1 | 4 | | 1.76 |
| 15415,90 | Spur Crater (15) | Anorthosite (F) | x | x | | x | | | | 4 | | 1.59 |
| 15684,4 | Station 9A (15) | Basalt | x | x | | | x | | | 1 | 3 | 3.41 |
| 60015,114 | ~30 m from LM* (16) | Anorthosite | x | x | x | | | | | 6 | | 6.76 |
| 60025,230 | ~15 m from LM (16) | Anorthosite | x | x | x | | | | | 3 | | 1.53 |
| 60055,4 | ~170 m from LM (16) | Anorthosite | x | x | | | | | | 6 | | 0.89 |
| 60215,13 | Station 10 (16) | An breccia | x | x | x | x | | | 1 | 4 | | 1.52 |
| 60618,4 | ~70 m from LM (16) | Anorthosite | x | x | | x | | | | 5 | | 2.41 |
| 60619,2 | 70 m from LM (16) | Anorthosite | x | | | | | 6 | 3 | | | 0.75 |
| 60629,2 | Near LM (16) | Anorthosite (F) | x | x | | x | | | | 3 | | 3.26 |
| 62237,21 | Buster Crater, St. 2 (16) | Anorthosite (F) | x | x | | | | | 2 | 15 | | 1.62 |
| 67075,41 | North Ray Crater (16) | Anorthosite (F) | x | x | | x | | | 1 | 4 | | 1.47 |
| 67415,113 | North Ray Crater (16) | Anorthosite (N) | x | x | | | | 1 | 5 | 1 | | 0.89 |
| 67746,12 | North Ray Crater (16) | Anorthosite (N) | | x | | | | | 6 | | | 0.57 |
| 68035,6 | Station 8 (16) | Anorthosite | x | x | | x | | | | 7 | | 3.12 |
| 69955,27 | Station 9 (16) | Anorthosite | x | x | x | | | | | 6 | | 4.99 |
| 69955,29 | Station 9 (16) | Anorthosite | x | x | x | | | | | 6 | | 5.13 |
| 73215,193 | Lara Crater (17) | Impact melt breccia | x | x | | | | 1 | 1 | 5 | | 3.41 |
| 76335,55 | Station 6 (17) | Anorthosite (M) | x | x | | | | | | 6 | | 1.97 |
| 79155,58 | Station 9 (17) | Gabbro | x | x | | | x | | | | 6 | 4.81 |

Abbreviations: LM=Lunar Module; F=Ferroan; M=Magnesian; N=Noritic; An=Anorthosite

*Probable collection location, but details of its collection, situation, and orientation are not known.

Table 2. Average FWHMχ measurements across all Miller indices for optical groups.

| | | Average FWHMχ (°χ) | | | | Number of Spots | |
|---|---|---|---|---|---|---|---|
| O.G. | Description | Apollo | s.d. | Mistastin | s.d. | Apollo | Mistastin |
| A | Uniform extinction | 0.79 | 0.32 | 0.67 | 0.23 | 16 | 8 |
| B | Slight undulose extinction | 0.93 | 0.40 | 0.89 | 0.46 | 10 | 18 |
| C | Undulose extinction | 2.58 | 2.03 | 1.07 | 0.80 | 65 | 15 |
| D | Partially isotropic | 3.14 | 1.39 | 2.54 | 1.77 | 8 | 8 |
| E | Diaplectic glass | N/A | | N/A | | N/A | N/A |

Abbreviations: O.G.=Optical Group; s.d. = standard deviation (1σ); N/A = Not applicable